Dependence of solar cell ESD voltage threshold on cover glass secondary emission properties

Sébastien L G Hess, Denis Payan, Pierre Sarrailh

Dependence of Solar Cell ESD Voltage Threshold on Cover Glass Secondary Emission Properties

Sébastien L.G. Hess, Denis Payan, and Pierre Sarrailh

***Abstract*— Spacecraft interacts with the charged particles of the space environment, leading to their electrostatic charging. This charging depends on the surface materials and their exposure to space. Thus, it is different for different parts of the spacecraft. This differential charging is particularly important on solar panels, which are composed of various polarized elements juxtaposed over small distances. This leads to strong electric fields ultimately leading to electrostatic discharges (ESDs), themselves being the onset of destructive secondary arcs. Hence, controlling the onset of ESDs is a key factor to prevent damages on spacecraft. Two ways are generally envisioned to act on the ESD onset: the geometry of the solar cells and the material electrostatic properties. In this article, the control of the ESD onset is tackled through the study of the effects of the cover glass secondary emission properties on the voltage threshold of solar cell ESDs. This study is conducted numerically with the spacecraft plasma interaction software (SPIS)-ESD software, as the natural variability of physical samples and the impossibility to have materials with controlled characteristics render the experimental study unpractical, if even feasible.**

***Index Terms*— Electrostatic discharge (ESD), numerical simulation, secondary electron yield, spacecraft charging.**

I. Introduction

SPACECRAFT collect and emit charged particles from and to the space environment. Depending on the exposure to space and on the material properties, different surfaces may end up having different electric potentials. Solar cell assemblies are particularly important sites for differential charging, as solar cells are composed of various materials with different characteristics and polarizations. In the most unfavorable conditions, such as that encountered by the SCATHA spacecraft [1], [2] on which the ECSS-E-ST-10-04C worst case is built [3], this differential charge between adjacent elements of the solar cell assembly could, theoretically, reach up to 5 kV between the dielectric cover glass and the underlying cell [4], [5]. In this case, the dielectric is positively charged relative to the underlying conductor due to the strong negative charge of the spacecraft ground and to the high photo and secondary electron emission yields of the cover glass facing the sun. Such a configuration is known as an "inverted potential gradient" configuration.

In practice, however, such high electric potential differences are unlikely. Given that the potential difference arise over a distance which is roughly equal to the dielectric thickness ($\sim$100 μm), the electric field at the border of the dielectric, conductor, and plasma—the so-called triple point—may reach several 10^7 V·m^{-1}, which is enough to give birth to electrostatic discharges (ESDs) between the conductor and the dielectric. In practice, discharges occur for potential differences of a few hundred volts.

Several models have been developed to explain the onset of ESDs on solar array [6], [7], [8], [9], [10]. Parks et al. [6] proposed that primary electrons are extracted from the conductor at the triple point due to the important electric field, as modeled by Fowler and Nordheim [11]. In addition, Williams and Williams [12] showed evidences of the impact of surface roughness on the ESD onset, with electric field amplification due to surface irregularities estimated between 100 and 1000.

Thus, the Fowler–Nordheim model for the field emission can be written as

$$J_{\mathrm{FN}} \propto \frac{\beta^2 U^2}{\phi_w \lambda^2} \exp\left(-v \frac{4\sqrt{2m}\lambda \phi w^{3/2}}{3\beta e\hbar U}\right) \tag{1}$$

with U the potential difference, λ the thickness of the cover glass, ϕ_W the metal work function, and $-e$ and m the electron charge mass. β is the field amplification factor due to surface irregularities and v is a correction factor for the Schottky–Nordheim barrier, which value is about 0.5 following [13] for the electric fields considered at ESD onset.

Emitted electrons gain energy due to the voltage gradient and impact the dielectric cover glass. Then, the energy released by the electron impacts produces a secondary electron emission. The secondary electron emission current can be written as

$$J_{\mathrm{sec}} = Y_{\mathrm{eff}} J_{\mathrm{FN}} \tag{2}$$

with Y_{eff} an effective electron emission yield, averaged on the primary electron incidence angles and energies over the cover glass edge. This yield includes both the contribution of backscattering (the incident electron "bounces" on the material interface) and of "true" secondary emission (an electron is

Manuscript received 13 September 2022; revised 21 December 2022; accepted 8 February 2023. This work was supported in part by the CNES Research and Technology Activity under Grant 4500063512 and in part by the ONERA Research (update of the spacecraft plasma interaction software (SPIS-ESD)) under Project 24003. The review of this article was arranged by Senior Editor S. T. Lai. *(Corresponding author: Sébastien L.G. Hess.)*

Sébastien L.G. Hess and Pierre Sarrailh are with ONERA, The French Aerospace Lab, F31400 Toulouse, France (e-mail: sebastien.hess@onera.fr).

Denis Payan is with CNES, F31400 Toulouse, France.

Color versions of one or more figures in this article are available at https://doi.org/10.1109/TPS.2023.3250712.

Digital Object Identifier 10.1109/TPS.2023.3250712

emitted from the material due to the incident electron energy deposition).

For energies of a few hundred electronvolts, the secondary electron emission yield, Y_{eff}, is larger than one, leading to the increase of the electric potential and to the electric field enhancement at the triple point vicinity. This starts a divergent process, in which the potential difference increases continuously together with the current of emitted electrons. Cho and Hastings [10] and Girard et al. [14] modeled the inverted potential gradient situation and showed that the combination of field emission and secondary emission by electron bombardment leads to an exponential electron current growth, up to some microamperes.

The onset process of the ESDs on solar cell assembly has been modeled numerically with spacecraft plasma interaction software (SPIS) [15], [16], [17], [18] by Girard et al. [14] and with a much more detailed physics model by Sarrailh et al. [19]. The SPIS-ESD software is based on the SPIS software developed in Europe to compute the surface charging of objects exposed to space plasma. In addition, it includes advanced numerical schemes and physical models for the Fowler–Nordheim emission and for the field enhancement on surface irregularities that allows modeling the onset of the ESD.

Sarrailh et al. [19] conducted a series of experiments of ESD onsets in a vacuum chamber under several different conditions and compared them to numerical simulation, which allowed to successfully validate the SPIS-ESD modelings. The authors used controlled experimental mock-ups of solar cells with controlled materials and geometries. This allowed them to highlight the effect of some key parameters, among which the conductor work function that controls the primary electron emission by Fowler–Nordheim effect, as expected from 1, and the dielectric surface conductivity.

The dependence on surface conductivity was understood as the impossibility for the electric potential to increase locally due to the charge dispersal by conduction at the surface of the dielectric: if the surface conduction current, J_{cond}, is larger than the charging current, the electrostatic potential does not increase and the divergent process cannot take place. The ESD onset condition requires that the secondary current dominates the two others

$$\boldsymbol{J}_{\text{sec}} - \boldsymbol{J}_{\mathbf{FN}} > \boldsymbol{J}_{\text{cond}}. \tag{3}$$

However, the impact of secondary emission parameters was not tested. Experimentally, it would require having enough different materials with electrostatic properties such as it is possible to test the effect of a single parameter with all other parameters being kept constant. In practice, this is complicated if not impossible. We thus chose to investigate the effect of the material properties numerically using SPIS-ESD. Our goal is to investigate separately the effect of the material surface conductivity and of the secondary emission yield.

We first present the SPIS-ESD numerical scheme, the simulation domain, and the simulation procedure. Then, we investigate the effect of varying the surface conductivity and the secondary emission yield. Finally, we discuss and conclude on the relative importance of these parameters.

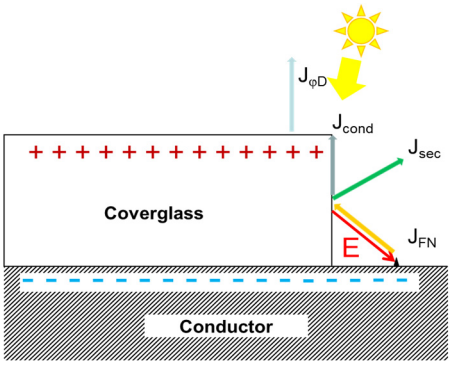

Fig. 1. Simple sketch of the geometry and currents for the cover glass charging and ESD onset for the interconnect geometry. Arrows stand for electron fluxes (hence oriented opposite to the currents).

II. Spacecraft Plasma Interaction Software-ESD

The SPIS-ESD simulation software [19] is based on the SPIS [15], [16], [17], [18], [20]. SPIS is an open-source simulation code developed by ONERA and Artenum with support from the ESA, CNES, and the Spacecraft Plasma Interaction Network in Europe (SPINE) Community to simulate the physics of charging and its effects on spacecraft.

SPIS computes the potential of spacecraft surfaces based on the current balance on and between each spacecraft surface elements. These currents are due to plasma collection, secondary particle emissions, emission of charged particles by active artifacts (electric thrusters, cathodes, etc.), and onboard electronics that may generate current or voltage differences between elements.

For simple configurations, this could be solved through analytic approximations of the plasma collections. However, SPIS also embeds a multimodel plasma simulation code that allows the accurate computation of the plasma currents collected on the surfaces, taking into account the geometrical configuration and plasma out of local thermal equilibrium.

SPIS-ESD extends the SPIS capabilities both by an improvement of the circuit solver that allows to handle the charging of the dielectrics on characteristic time scale of minutes and the discharge phenomena occurring with characteristics time scales of nanoseconds and by introducing the physical processes involved in the discharge (Fowler–Nordheim emission, field enhancement by metal irregularity, metal vaporization and ionization, etc.).

In this article, we limit ourselves to a configuration simulating the ESD onset on an interconnect, which is represented in Fig. 1 together with the main currents participating to the ESD. A typical SPIS-ESD simulation describes a slice of solar cell in a simulation domain of $0.5 \times 4 \times 4$ cm (see Fig. 2). The cell surface stands at the bottom of the simulation domain, while open environment boundary conditions are applied at the opposite top surface. The boundary conditions on the sides of the simulation domain are set reflective.

The geometry represents a 100-μm layer of cover glass covering a metallic surface on the bottom side of the simulation domain, except for a small (2 mm long) region, where the metal is left uncovered. The spot itself is a 0.1×0.1 μm surface on the metal, sitting 0.1 μm away

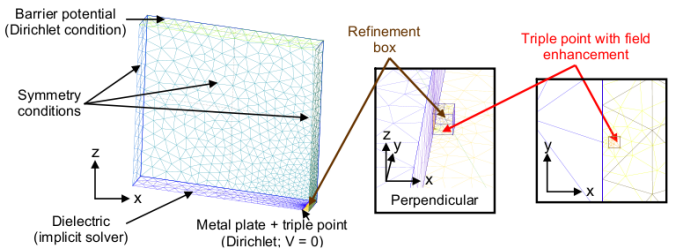

Fig. 2. Simulation domain and mesh refinement close to the triple point for a SPIS-ESD simulation.

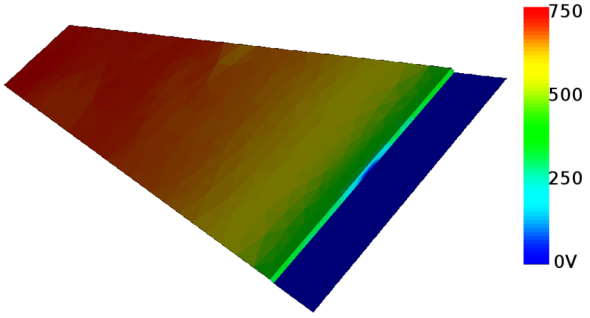

Fig. 3. Surface potential simulated by SPIS with $Y_0 = 4$, $E_{max} = 200$ eV, $\mathbf{R}_{\square} = 5{\cdot}10^{15}\Omega\square$, and a potential bias of 750 V.

from the triple point in which the Fowler–Nordheim effect can be amplified due to (unmeshed) surface irregularities. The mesh size is a fraction of centimeter, but the mesh is refined to submicrometer scales in a region close to the triple point.

A potential difference is applied between the conductor (whose potential is fixed at 0 V) and the environment boundary conditions at the top of the domain. A solar UV flux is set as part of the environment condition to charge the cover glass surface (see Fig. 3). Because of the low photoelectron temperature (set to 2 eV in the SPIS-ESD simulations), the escaping photoelectron current tends to charge the cover glass surface at a potential close to that of the environment (within a few volts) before being limited by the photoelectron recollection.

To determine the threshold, we proceed by increasing gradually the potential difference between the environment and the underlying conductor by steps of 50 V. Each step stands for a duration of 50 s.

The current emitted by the spot increases exponentially at the ESD onset. This further leads to a heating of the metal irregularity in the spot, an outgassing of the material, and an ionization of the outgassed atoms. At this stage, a stable cathode spot is set and a diffuse arc occurs [21]. SPIS-ESD simulates the heating and the outgassing due to a thermic model and considers that an ESD occurs when the mean free path of atoms before ionization is lower than the size of the domain. Simulating the cathode spot and the physics of arcs is out of the scope of SPIS-ESD.

III. ESD Threshold Dependence on Resistivity

We first simulate the ESD onset in a geometrical configuration that models the discharge from a metal irregularity on an interconnect to the charged cover glass. In this configuration, the dielectric lies on an "infinite" conductive ground surface. This configuration, with an infinite ground plane, allows the analytical computation of the capacitance of each dielectric surface element [19]. The geometry of the simulation is shown in Fig. 2.

TABLE I
Reference Material Parameters

Parameter	Material	
	Conductor (Ag)	*Dielectric*
SEEE maximum yield at 0° incidence δ_{max}	2.2	4 (0.5 – 20)
Energy for the maximum yield E_{max}	350 eV	200 eV (100 – 500 eV)
Photo-emission current J_φ	3.10^{-5}A/m^{-2}	2.10^{-5}A/m^{-2}
UV incidence angle θ	12°	
Surface resistivity $R_\square$	0 Ω	5.10^{15} Ω (2.10^{16} - 5.10^{15} Ω)
Work function ϕ_W	4.23	-
Amplification factor β	800	-
Thickness λ	-	100 µm

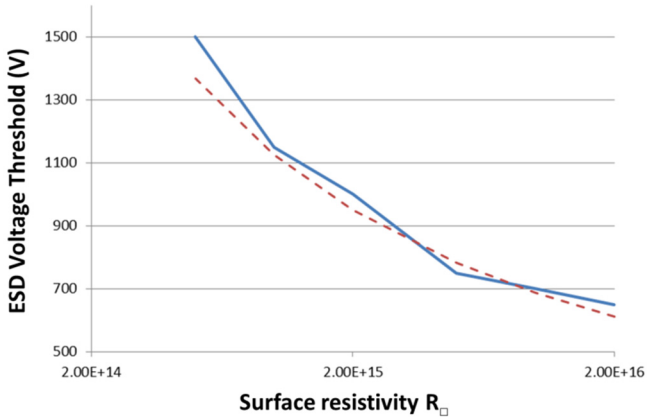

Fig. 4. ESD voltage threshold versus the cover glass surface resistivity in Ω□. The solid curve stands for simulation results, and the dashed one for the simple model of the current balance [(1), see details in the discussion].

The reference cover glass and metal properties are given in Table I. Then, we modify individually each property to investigate their impact on the ESD threshold.

We first perform a set of simulation to investigate the variation of the ESD voltage threshold with the dielectric surface conductivity, in an attempt to retrieve the results of Sarrailh et al. [19]. All simulations were performed in the same conditions with the same parameters, except for the surface resistivity that varies from $5{\cdot}10^{14}$ to $2{\cdot}10^{16}$ Ω□.

The results are displayed in Fig. 4. The ESD threshold varies from 1500 V for low resistivity down to 600 V for larger resistivity, in agreement with [19]. The increase of the voltage threshold with surface conductivity is understood as a leakage current on the surface that prevents the local increase of the potential on the cover glass edge due to the secondary electron emission. The red curve corresponds to a simplified model of the current balance on the cover glass edge (3). The details of the models are discussed in Section V.

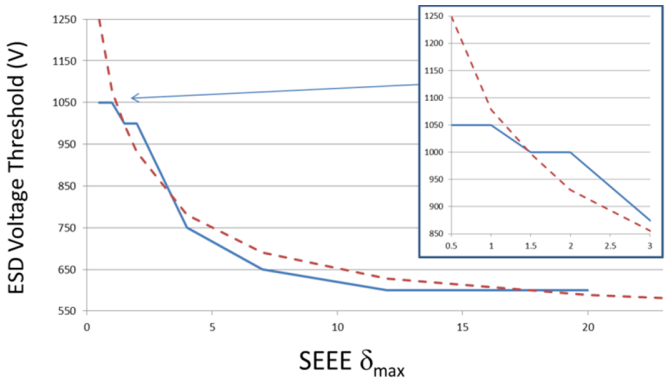

Fig. 5. ESD voltage threshold versus secondary electron maximum electron yield. The larger is the yield, the lower is the threshold voltage. The blue solid curve stands for simulation results, and the red dashed curve for the simple model.

IV. ESD Threshold Dependence on SEEE Parameters

Then, we investigate the effect of secondary electron emission parameters, starting with the maximum electron yield at normal incidence $\delta_{\max}$. As the secondary emission is responsible for the nonlinear current amplification process in the ESD phenomenon, it is expected that a larger $\delta_{\max}$ leads to a smaller voltage threshold. We simulated $\delta_{\max}$ values between 0.5 and 20, with a peak for an incident electron energy $E_{\max} = 200$ eV. The results are displayed in Fig. 5.

The ESD voltage threshold evolves with $\delta_{\max}$ as expected, with a minimum value of 600 V for large yields ($\delta_{\max} > 10$). The ESD voltage threshold increases rapidly for yields smaller than $\delta_{\max} = 5$ toward values larger than 1000 V.

More surprisingly, ESDs occur even for the values of $\delta_{\max}$ smaller than 1. This is due to two effects: first, the actual yield depends on the incidence angle, which is large in our case, leading to larger yields; second, the yield does not account for backscattering of electrons, which tends toward 1 for tangential incidence angle. Hence, it is possible to get ESDs even with a cover glass material which maximum yield at normal incidence, $\delta_{\max}$, is 0.5.

The second parameter controlling the secondary electron emission is the energy of the incident electron corresponding to the maximum of the emission yield, $E_{\max}$.

Contrary to the other parameters, this material characteristic does not have a monotonic effect on the ESD voltage threshold, as shown in Fig. 6. The threshold reaches a minimum for $E_{\max} = 200$ eV. The energy of the minimum, $E_{\max,}$ does not change with the maximum yield value, $\delta_{\max}$.

This is understood as being due to the fact that the secondary emission current must not be considered locally, but over the whole side of the cover glass, with electron energy ranging from nearly 0 eV, up to the energy corresponding to the maximum potential on the side of the cover glass.

When $E_{\max}$ is larger than the maximum energy gained for the incident electrons, the secondary emission is less efficient, explaining why the ESD voltage threshold increases for larger values, but for small values of $E_{\max}$, a large part of the incident electrons have energy larger than $E_{\max}$ and the secondary emission yield decreases too.

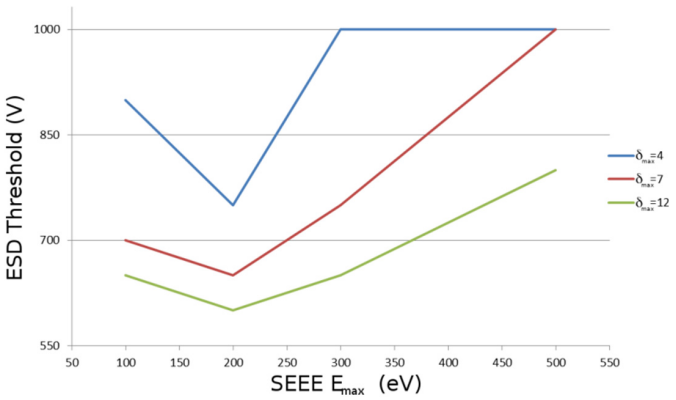

Fig. 6. ESD voltage threshold versus $E_{\max}$ for $\delta_{\max} = 4$, 7, and 12.

Taking into account the effect of the incidence angle, it is possible to compute that for a simple Vaughan law, the maximum averaged yield is obtained for $E_{\max}$ close to the third of the maximum potential. In our simulation, this maximum potential is between 600 and 750 V for the optimal $E_{\max}$ value ($\delta_{\max}$ between 2 and 4). Thus, the optimum $E_{\max}$ should be between 200 and 250 eV, which is consistent with the simulation results.

V. Discussion

Our simulations show that the secondary electron emission parameters play a role of similar amplitude than the surface resistivity on the control of the ESD threshold voltage. This can be understood in terms of current balance on the cover glass edge. Indeed, the ESD process requires that above some threshold voltage difference between the cover glass surface and the conductor, the current due to secondary electron emission overcomes the neutralizing currents, among which the primary electron current and the surface conduction current (see Fig. 1). The Fowler–Nordheim model for the field emission is given by (1), where the field amplification factor, β, is taken equal to 800 in our modeling.

The effective electron emission yield, Y_{eff}, depends on the incidence angle, the retrodiffusion coefficient, and some average over the incident energy, as highlighted by the dependence of the voltage threshold on $E_{\max}$ (see Section III). When the potential difference is sufficient to trigger ESDs, Y_{eff} can be estimated about $2\delta_{\max}$ for large $\delta_{\max}$ and $E_{\max} \sim 200$ eV, tending toward the efficiency of electrons having the optimal incident energy and a grazing incidence. On the contrary, Y_{eff} is about 1 for small $\delta_{\max}$, corresponding to retrodiffusion at small incidence angle. These are very crude considerations but they allow retrieving correct estimates of the ESD voltage thresholds. For this reduced model, we assumed an effective yield $Y_{\text{eff}} = (1 + 4\delta_{\max}^2)^{1/2}$.

To determine the thresholds, one must also estimate the conduction current that we model as

$$\boldsymbol{J}_{\text{cond}} \propto \frac{U\sigma_{\square}}{\lambda^2} \tag{4}$$

with $\sigma_{\square}$ the surface conductivity of the cover glass. The ESD onset condition, (3), can be rewritten as

$$\boldsymbol{A}\frac{\beta^2 U}{\phi_W \sigma_{\square}}(\boldsymbol{Y}_{\text{eff}} - 1)\mathbf{exp}\left(-\boldsymbol{v}\frac{4\sqrt{2m}\lambda\phi w^{3/2}}{3\beta e\hbar U}\right) > 1 \tag{5}$$

with A a constant related to the effect geometry of the triple point on the Fowler–Nordheim emission and of the charge conduction on the cover glass surface. The fit of the results leads to a value about 10^{-23} A·eV/V^2.

We overplot the voltage threshold obtained with (5) in Figs. 4 and 5. The global trends of the ESD voltage threshold variation with the surface resistivity and with the maximum yield are reproduced.

VI. Conclusion

We simulated the onset of ESDs at the triple point between the plasma, the cover glass, and a metallic conductor in a configuration that is similar to that of interconnects between solar cells. The threshold voltage for the onset of the ESDs was determined for different material characteristics of the cover glass that control the surface resistivity and the secondary electron emission yield. We find that the ESD voltage threshold decreases when the surface resistivity increases or when the maximum electron yield increases. While the effect of surface resistivity was already documented [19], the dependence on the maximum yield is a new finding. Nevertheless, such dependence was expected and can be modeled by the current balance on the cover glass edge.

More surprisingly, the energy of the incident electrons for which the secondary electron emission is maximum, $E_{\max}$, presents a nonmonotonic effect on the ESD voltage threshold. This is interpreted as a consequence of the integration of the secondary emission yield over the whole thickness of the cover glass. For large $E_{\max}$, the electrons emitted by the conductor do not gain enough energy to generate secondary electrons with the maximum efficiency. For small $E_{\max}$, many incident electrons have energies larger than the energy providing the maximum efficiency and the integrated yield decreases. The value of $E_{\max}$ providing the lowest voltage threshold is about 200 eV.

Although we argue that the ESD voltage threshold is governed by the balance of the currents, we explore the effects of all current but one: the photocurrent. Preliminary work showed interesting effects but required more investigation and is out of the scope of this article. Nonetheless, a future accurate model of the ESD voltage threshold must take into account this current and its effect on the voltage profile of the cover glass border more properly that we do in this article.

References

[1] M. Gussenhoven and E. Mullen, "A 'worst case' spacecraft charging environment as observed by SCATHAon 24 April 1979," in *Proc. 20th Aerosp. Sci. Meeting*, Jan. 1982, p. 271, doi: 10.2514/6.1982-271.

[2] W. Schnuelle, "Charging analysis of the SCATHA satellite," in *Proc. Spacecraft Charging Technol. Conf.*, 1978, pp. 123–143.

[3] *Space Engineering–Space Environment*, ECSS, ESA Requirements Standards Division, ESTEC, Noordwijk, The Netherlands, 2008.

[4] J.-C. Matéo-Vélez et al., "Simulation and analysis of spacecraft charging using SPIS and NASCAP/GEO," *IEEE Trans. Plasma Sci.*, vol. 43, no. 9, pp. 2808–2816, Sep. 2015, doi: 10.1109/TPS.2015.2447523.

[5] J.-C. Matéo-Vélez, A. Sicard, D. Payan, N. Ganushkina, and N. P. Meredith, "Spacecraft surface charging induced by severe environments at geosynchronous orbit," *Int. J. Res. Appl.*, vol. 16, no. 1, pp. 89–106, 2018, doi: 10.1002/2017SW001689.

[6] D. E. Parks, G. A. Jongeward, I. Katz, and V. A. Davis, "Threshold-determining mechanisms for discharges in high-voltage solar arrays," *J. Spacecraft Rockets*, vol. 24, no. 4, pp. 367–371, Jul. 1987, doi: 10.2514/3.25926.

[7] D. E. Hastings, G. Weyl, and D. Kaufman, "Threshold voltage for arcing on negatively biased solar arrays," *J. Spacecraft Rockets*, vol. 27, no. 5, pp. 539–544, Sep. 1990, doi: 10.2514/3.26177.

[8] D. E. Hastings, M. Cho, and H. Kuninaka, "The arcing rate for a high voltage solar array: Theory experiment and predictions," *J. Spacecraft Rockets*, vol. 29, no. 4, pp. 538–554, 1992, doi: 10.2514/6.1992-576.

[9] D. Payan, F. Sverin, J.-P. Catani, J. F. Roussel, R. Reulet, and D. Sarrail, "Electrostatic discharges on solar arrays—Physical model of inverted potential gradient electrostatic discharge," in *Proc. 7th Spacecraft Charging Technol. Conf.*, 2001, p. 151.

[10] M. Cho and D. E. Hastings, "Computer particle simulation of high-voltage solar array arcing onset," *J. Spacecraft Rockets*, vol. 30, no. 2, pp. 189–201, Mar. 1993, doi: 10.2514/3.11527.

[11] R. H. Fowler and L. Nordheim, "Electron emission in intense electric fields," *Proc. Roy. Soc. London A, Containing Papers Math. Phys. Character*, vol. 119, no. 781, pp. 118–173, 1928, doi: 10.1098/rspa.1928.0091.

[12] D. W. Williams and W. T. Williams, "Effect of electrode surface finish on electrical breakdown in vacuum," *J. Phys. D, Appl. Phys.*, vol. 5, no. 10, p. 1845, Oct. 1972, doi: 10.1088/0022-3727/5/10/314.

[13] R. G. Forbes, "Simple good approximations for the special elliptic functions in standard Fowler-Nordheim tunneling theory for a Schottky-Nordheim barrier," *Appl. Phys. Lett.*, vol. 89, Aug. 2006, Art. no. 113122, doi: 10.1063/1.2354582.

[14] L. Girard, D. Payan, J.-F. Roussel, and F. Sverin, "SPIS modelling of electrostatic discharge triggering in a solarcell gap," in *Proc. 10th Spacecraft Charging Technol. Conf.*, 2007.

[15] J.-F. Roussel et al., "Design of a new modular spacecraft plasma interaction modeling software (SPIS)," in *Proc. 8th Spacecraft Charging Technol. Conf.*, Huntsville, AL, USA, 2003, pp. 1–15.

[16] J.-F Roussel, F. Rogier, D. Volpert, G. Rousseau, J. Forest, and A. Hilgers, "Spacecraft plasma interaction software (SPIS): Numerical solvers. Methods and architecture," in *Proc. 9th Spacecraft Charging Technol. Conf.*, Tsukuba, Japan, 2005, pp. 462–472.

[17] J.-F. Roussel et al., "SPIS open-source code: Methods, capabilities, achievements, and prospects," *IEEE Trans. Plasma Sci.*, vol. 36, no. 5, pp. 2360–2368, Oct. 2008, doi: 10.1109/TPS.2008.2002327.

[18] J.-F. Roussel et al., "SPIS multitimescale and multiphysics capabilities: Development and application to GEO charging and flashover modeling," *IEEE Trans. Plasma Sci.*, vol. 40, no. 2, pp. 183–191, Feb. 2012, doi: 10.1109/TPS.2011.2177672.

[19] P. Sarrailh et al., "Comparison of numerical and experimental investigations on the ESD onset in the inverted potential gradient situation in GEO," *IEEE Trans. Plasma Sci.*, vol. 40, no. 2, pp. 368–379, Feb. 2012, doi: 10.1109/TPS.2011.2179320.

[20] P. Sarrailh et al., "SPIS 5: New modeling capabilities and methods for scientific missions," *IEEE Trans. Plasma Sci.*, vol. 43, no. 9, pp. 2789–2798, Sep. 2015, doi: 10.1109/TPS.2015.2445384.

[21] L. Monnin, S. L. G. Hess, J.-F. Roussel, P. Sarrailh, and D. Payan, "Flash-over propagation simulation upon spacecrafts solar panels," *J. Appl. Phys.*, vol. 130, no. 22, Dec. 2021, Art. no. 223302, doi: 10.1063/5.0061320.